PAPER • OPEN ACCESS

A dynamical symmetry triad in high-harmonic generation revealed by attosecond recollision control

New Journal of Physics
The open access journal at the forefront of physics

Deutsche Physikalische Gesellschaft DPG
IOP Institute of Physics

Published in partnership with: Deutsche Physikalische Gesellschaft and the Institute of Physics

OPEN ACCESS

RECEIVED
28 November 2019

REVISED
21 March 2020

ACCEPTED FOR PUBLICATION
24 March 2020

PUBLISHED
5 May 2020

PAPER

A dynamical symmetry triad in high-harmonic generation revealed by attosecond recollision control

Sergey Zayko[1,5], Ofer Kfir[1,5,6], Eliyahu Bordo[2], Avner Fleischer[2,3], Oren Cohen[2] and Claus Ropers[1,4,6]

[1] University of Göttingen, 4th Physical Institute, Göttingen 37077, Germany
[2] Solid State Institute and Physics Department, Technion—Israel Institute of Technology, Haifa 3200003, Israel
[3] School of Chemistry, Tel Aviv University, Tel-Aviv 6997801, Israel
[4] International Center for Advanced Studies of Energy Conversion (ICASEC), University of Göttingen, Germany
[5] These authors contributed equally to this work.
[6] Authors to whom any correspondence should be addressed.

E-mail: ofer.kfir@phys.uni-goettingen.de and claus.ropers@uni-goettingen.de

Keywords: dynamical symmetry, high harmonic generation, emergent symmetries

Supplementary material for this article is available online

Abstract

A key element of optical spectroscopy is the link between observable selection rules and the underlying symmetries of an investigated physical system. Typically, selection rules directly relate to the sample properties probed by light, yielding information on crystalline structure or chirality, for example. Considering light-matter coupling more broadly may extend the scope of detectable symmetries, to also include those directly arising from the interaction. In this letter, we experimentally demonstrate an emerging class of symmetries in the electromagnetic field emitted by a strongly driven atomic system. Specifically, generating high-harmonic radiation with attosecond-controlled two-color fields, we find different sets of allowed and forbidden harmonic orders. Generalizing symmetry considerations of circularly polarized high-harmonic generation, we interpret these selection rules as a complete triad of dynamical symmetries. We expect such emergent symmetries also for multi-atomic and condensed-matter systems, encoded in the spectral and spatial features of the radiation field. Notably, the observed phenomenon gives robust access to chiral processes with few-attosecond time precision.

The concept of *emergence* describes the appearance of entirely new properties of a coupled system, which only arise from the interaction of its constituents. In light-matter interaction, emergent phenomena are particularly prominent in strongly driven states of matter, as evident in light-induced variants of superconductivity [1], the Hall effect [2], and topological insulators [3] in the condensed phase, as well as exceptional points in molecules [4, 5], Kramers–Henneberger states in gases [6, 7], and time-crystals in isolated many-body systems [8, 9]. Such emergent states are often governed by novel symmetry properties and topologies, which may be probed by external or emitted radiation fields. However, while much attention is drawn to the light-induced creation of novel states of matter, a wider scope should also include possible emergent states of the radiation field.

Here, we report on the experimental observation of an emergent class of symmetries in the electromagnetic field emitted by a strongly driven atomic system. Specifically, we analyze the sets of allowed and forbidden harmonic orders in high-harmonic generation from tailored bi-circular and bi-elliptical fields. Corroborated by theoretical modeling, the identified selection rules correspond to a complete triad of dynamical symmetries. We believe that the general principles underlying our observations will be equally relevant for other systems, including crystalline solids.

Spectral and polarization selection rules serve as direct measures for the symmetries of the underlying Hamiltonian and interaction [10, 11]. Canonical examples in linear and perturbative nonlinear probing are molecular analysis by Raman and infrared spectroscopy [12, 13] or selection rules in wave mixing and

harmonic generation [14–17]. Similarly, symmetry-breaking is widely used in surface-sensitive sum-frequency generation [18], second-harmonic imaging of multiferroic domains in solids [19], and high-order harmonic generation from atoms [20–22], molecules [23, 24] and solids [25–28].

For these parametric processes, the selection rules can be straightforwardly interpreted in the time-domain: the destructive interference between multiple light-emission events may lead to a group of forbidden emission frequencies (e.g. two events of equal amplitude and opposite phase). Breaking of the underlying symmetry or changing the timing of the emissions allows these spectral lines to appear. In the case of high-order harmonic generation (HHG), the separate emission events represent recollisions of an electronic wavepacket with an atomic or molecular parent ion [29, 30]. The recollision picture facilitates the retrieval of attosecond timing and orientation from spectral features in HHG, as exploited in measurements of the time structure of the tunneling process [31, 32], molecular tomography [33], and chiral discrimination [34, 35].

A particularly relevant example is the generation of circularly polarized high-harmonics of bi-circular laser fields in isotropic media, which ties the spectrum to the polarization state of the harmonics [36–39]. The bi-circular field, composed of a counter rotating fundamental field and its second harmonic, reaches its maximum amplitude three times in an optical cycle, where each of those is rotated by 120° in the polarization plane. A more general representation for the underlying link between temporal delays and rotations of the bi-circular driving field can be written as a three-fold dynamical symmetry, described in more detail in reference [38],

$$\vec{E}\left(t+\frac{T}{3}\right)=\bar{R}_{(120^\circ)}\vec{E}\,(t)\,. \tag{1}$$

Here, $\vec{E}\,(t)$ is the overall electric field in the system (both the incident bi-circular driving field and the emitted radiation), T is the period of the fundamental field and $\bar{R}_{(120^\circ)}$ is the operator for 120° rotation in the polarization plane. Equation (1) originates from the dynamical symmetry of the bi-circular driving laser: a left-rotating field with a cycle T overlaps with its counter-rotating second harmonic three times in an optical period, each of which at a rotated orientation. A temporal shift of $T/3$, is therefore, equivalent to a rotation by 120°. In an isotropic medium the resulting Hamiltonian inherits the driving field's symmetry, and thus, the emitted radiation complies with equation (1) as well. The symmetry in equation (1) imposes the distinct suppression of every third harmonic order, $q_{\mathrm{suppr}}=3m=\ldots 21,24,\ldots,45,48,\ldots$.(with integer m). Notably, the emitted harmonic orders are circularly polarized [36–39], if effects from the pulse envelope [20, 21, 40] can be neglected. This three-fold selection rule is presently considered unique, where only a specific set of harmonics is forbidden, and its suppression reveals the Hamiltonian symmetry [11].

Our experimental setup is schematically shown in figure 1. An amplified pulsed beam (Ti:sapphire laser, 800 nm central wavelength, 40 fs pulse duration, 2 mJ pulse energy) is modified by a MAZEL-TOV apparatus [41] into a bi-chromatic field, comprising the fundamental field and its second harmonic with equal intensities at the focus. A tilted glass plate (0.15 mm, fused silica) tunes the bi-chromatic phase, which is the relative phase between the two driving fields. The initial polarization of the two colors is linear, where the second harmonic field is perpendicular to the fundamental. The final polarization state (see inset of figure 1) is controlled by a quarter-wave plate (QWP) for both 800 nm and 400 nm, comprising quartz and MgF_2 slabs. Rotation of the QWP tunes the two-color polarization states from counter-rotating circular at an angle of 45°, through equal ellipticities with perpendicular major axis, and back to the original perpendicular linear polarizations at QWP angles of 0° or 90°. Thus, the polarization is orthogonal in terms of Jones-vector calculus [42] throughout the experiment [see figure 1(b)]. The two colors co-focus in a He-filled gas cell, and the generated high-order harmonic spectrum is analyzed by a toroidal grating and a charge-coupled device (CCD) camera. The spectrum image in figure 1(c) shows the established suppression of every third harmonic order, imposed by the three-fold dynamical symmetry of equation (1).

Beyond this well-known suppression of the $q=3m$ harmonics by bi-circular fields [36–39, 53], upon controllably varying the bi-elliptical incident polarization state, we have discovered two additional three-fold selection rules, corresponding to the suppression of either the $3m+1$ or the $3m+2$ harmonics. Figure 2(a) plots experimental spectra for selected bi-chromatic phases, and a quarter-wave plate angle of 38°, corresponding to an ellipticity of 0.78 (ratio of minor to major ellipse-axes) for each of the driving fields. These spectra clearly show that the suppression of every third harmonic order can be shifted in a controllable manner among the sets given by $q_{\mathrm{suppr}}=3m, 3m+1, 3m+2$. The three sets of selection rules can be generalized as the emergence of a family of three dynamical symmetries, that is, a triad,

$$\text{Generalized symmetry}:\vec{E}\left(t+\frac{T}{3}\right)=\mathrm{e}^{\mathrm{i}\frac{2\pi}{3}n}\bar{R}_{(120^o)}\vec{E}\,(t)\,, \tag{2}$$

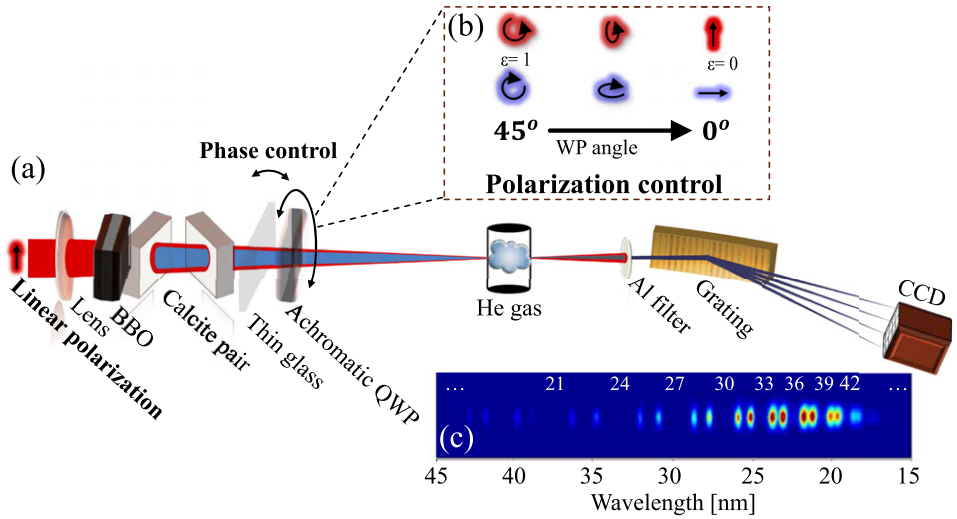

Figure 1. Outline of the experiment. (a) A bi-chromatic beam tailored by a MAZEL-TOV apparatus (see text) generates HHG in a He-filled gas cell. The driving laser is blocked by an aluminum filter, while the HHG is spatially dispersed by a toroidal grating and recorded on a CCD. (b) The relative phase and polarization state of the fundamental laser beam (red) and its second harmonic (blue) are controlled by the tilting of a thin glass slab and by the rotation of an achromatic quarter-wave plate (QWP), respectively. The polarization of the two spectral components is tuned from counter-rotating circular, through counter-rotating elliptical, with equal ellipticity and perpendicular major axis, to perpendicular linear polarization. (c) The HHG beamlets as recorded on the CCD for a bi-circular field demonstrate the suppression of every third harmonic order. White numbers indicate the suppressed harmonic orders.

with the triad index, $n = 0, 1, 2$. Here, $\vec{E}(t) = \sum_q \vec{E}_q e^{iq\omega_0 t}$ is the complex representation of the electric field at a given position, the real part of which is the physical field, where $\omega_0 = 2\pi/T$ is the fundamental angular frequency. The additional phase term, $e^{\frac{2\pi i}{3}n}$, generalizes equation (1) ($n = 0$) to the full triad of dynamical symmetries, where the index n can be controlled by tuning the experimental parameters, such as the ellipticity and the bi-chromatic phase (see additional details in the supplementary). Unlike the harmonic emission that obeys equation (1), where the dynamical symmetry is imposed by the bi-circular driving field, the symmetry expressed in equation (2) applies neither to the Hamiltonian nor the driving bi-elliptical field. Thus, the bandwidth of such a symmetry equation is inherently limited. Low frequencies such as the fundamental field and its second harmonic cannot comply with this symmetry. It is surprising, though, that this emerging symmetry applies to a large bandwidth. The experimental spectrum marked red in figure 2(a) shows a selection rule that correspond to equation (2) over the entire observable spectrum, in the range of 20 to 45 harmonic orders (photon energies of 30–70 eV, respectively). The bi-chromatic phase governs whether the $3m + 1$ (red) or the $3m + 2$ [green line in figure 2(a)] harmonics are suppressed.

Figure 2(b) presents the HHG spectrograms recorded by continuously tuning (sweeping) the quarter-wave plate for two bi-chromatic phases [determined to be about 0.1π and 0.7π by comparison with simulations presented in figure 3(d)]. The case of a bi-circular field with a QWP angle of 45°, is identified by the distinct suppression of harmonic orders $q_{\text{suppr}} = 3m$ (e.g., see suppressed harmonic $q_{\text{suppr}} = 39$, dashed black line). The selection rule for the triad index $n = 0$, as in equation (1), is robust in the sense that it directly follows from the three-fold dynamical symmetry of the incident field (with the isotropic medium) and covers all frequencies. It is therefore independent of the relative phase between the two fields or the relative power. As soon as the quarter-wave plate is detuned from 45°, the field becomes bi-elliptical, the three-fold symmetry of the driving field is broken, and the suppressed harmonics reappear. Additionally, the cutoff extends due to the generally larger field amplitudes for elliptically polarized fields, compared to circularly polarized fields. At a few-degree offset from circular polarization, namely at QWP = 38°, a different three-fold symmetric spectrum emerges, with characteristic suppressions of every third harmonic order.

To understand the microscopic origin of the new three-fold symmetries we turn to consider the attosecond emission events contributing to the HHG [43, 44]. In the case of a bi-circular driving field, for which equation (1) applies, the HHG radiation can be represented in time domain as a triplet of rotated attosecond pulses, equally spaced within an optical cycle, as illustrated in figure 3(a). Introducing bi-elliptical polarization leads to changes in both the recollision timing, Δt, and the phase, $\Delta\phi^{\text{intr}}$ of each burst separately [see figure 3(b)]. Slight changes in the timing and phase of the three bursts have drastic

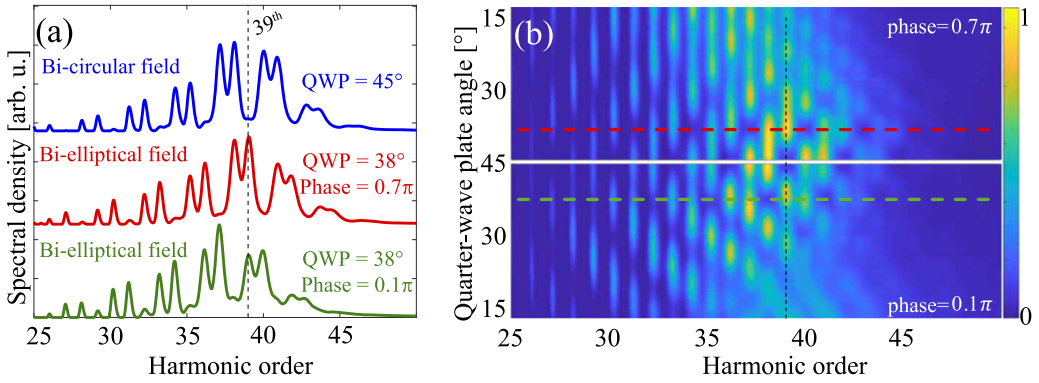

Figure 2. Spectra exhibiting emergent three-fold symmetries. (a) Controlling the set of suppressed harmonic orders, $q_{\mathrm{suppr}} = 3m, 3m+1$ and $3m+2$, colored blue, red and green, respectively. m is an integer. (b) HHG spectral density (linear scale) vs the angle of the quarter-wave plate, for relative phases of 0.1π and 0.7π between the two colors. The phases for the upper and the lower spectrograms are estimated from fits to the simulations. For a bi-circular driving field (QWP = 45°), the spectrum is independent of the relative phase. However, the phase determines which of the harmonic orders are suppressed for a bi-elliptical field. The dashed green and red lines mark the parameters for the corresponding spectra in (a). A vertical dashed line marks the 39th harmonic order.

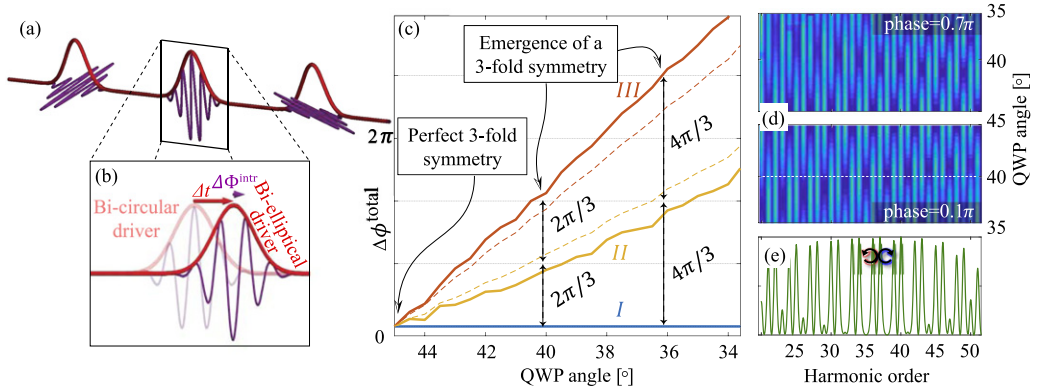

Figure 3. The attosecond origin of the emerging selection rules. (a) An illustration of the three subsequent attosecond emission events, tilted by 120°, as for a bi-circular driving field. (b) Tuning the QWP induces a temporal delay, Δt, and an intrinsic phase shift, $\Delta\phi^{\mathrm{intr}}$, to each pulse, originating from the trajectory of the laser-driven electron (details in the supplementary). (c) The overall phase of every attosecond pulse, $\Delta\phi^{\mathrm{total}} = q\omega_0\Delta t + \Delta\phi^{\mathrm{intr}}$, vs the QWP angle, for a bi-chromatic phase of 0.7π. At particular QWP angles (vertical arrows), the phase is near a multiplicity of $2\pi/3$, which yields an emergent symmetry (see equation (2) and the supplementary). The effect of the temporal phase alone, $q\omega_0\Delta t$, is shown in dashed lines. (d) Simulated spectral density vs the QWP angle, for different bi-chromatic phases. The white dashed line marks the parameters for the simulated spectrum shown in (e).

effect on the spectrum and polarization of the emitted harmonics, even for changes that correspond to a fraction of an optical cycle.

Using semi-classical simulations for HHG driven by equal bi-chromatic intensities, we follow the phase of the 39th harmonic order for a varying QWP angle (see figures 3(b) and (c)). For these simulations, we find the three electron trajectories during one fundamental optical cycle, in which the electron returns to the origin with a kinetic energy that corresponds to the emission of the selected harmonic order. For each trajectory, we find the initial transverse velocity of the electron, the ejection and recollision times, and the position and kinetic energy along the path. We follow each of these trajectories for varying ellipticity (i.e. QWP angle) and bi-chromatic phases. The orientation, timing, and the intrinsic-phase accumulated during the electron quiver is then used to analyze the HHG radiation (see figure 3). In the case of a bi-circular driving field, the field's properties, e.g., the maximal amplitude, repeats every third of the optical cycle. When the QWP is detuned from 45°, the peaks of the field are no longer at an equal temporal spacing along the optical cycle. Thus, a particular recollision event can occur later, compared with the bi-circular

case, due to delays in the field that brings the electron trajectory back to the origin. Earlier ionization times also correlate with delayed recollisions. In a simplified picture, the intrinsic phase relates to the time the electron spends in the continuum, between its tunnel-ionization and the final recombination. Thus, $\Delta\phi^{\mathrm{intr}}$ is inversely correlated to the ionization timing. More accurately, however, the phase is given by the path integral over the entire electron trajectory [30, 45–47]. Thus, an imbalance between the laser's electric-field amplitudes during the three trajectories also contributes to a difference in their intrinsic phases. While the dominant contribution to the overall recollision phase is the relative delays, Δt [dashed lines in figure 3(b)], the intrinsic phases provide for important corrections. Specifically, the phase corrections for the first and second recollisions are opposite, reducing and increasing the overall phase of the adjacent recollisions, with respect to a reference recollision. Importantly, for specific bi-chromatic phases, adjacent recollisions acquire an approximately equal phase difference, which simply scales linearly with the QWP rotation (figure 3(c)). At a particular QWP angle, the radiation phases differ by exact multiples of $2\pi/3$ [see arrows in figure 3(c)]. Thus, the additional phase of $2\pi/3$ between recollisions separated by a delay of $T/3$ is the origin of the term $\mathrm{e}^{\frac{2\pi i}{3}n}$ in equation (2). The simulation shows that the recollision orientations remain separated by 120° approximately, so its contribution is negligible [see figure S.3(b) in the supplementary]. In the experiment, the emerging selection rules are found for a QWP angle of 38°, which slightly deviates from the values found by the semi-classical simulations, possibly due to the effect of the screened Coulomb potential [48, 49]. The nearly linear relationship between the QWP angle and the suppressed harmonic orders in the experimental spectrogram (figure 2(b)) suggests that for multiple harmonic orders, the tuning of the QWP induces approximately equal relative phases between the recollisions. Indeed, our simulations reproduce this observation, predicting that the phase differences of the three recollisions scale similarly with the QWP rotation for multiple harmonics (see figure S.3 in the supplementary). As with equation (1), the emerging symmetries of equation (2) constrain the harmonics to be circularly polarized. Both numerical simulations and the repeating of the experiment in Ne gas, utilizing chiral p-orbitals [24, 50–52, 54], indicate that the unsuppressed harmonics are circularly polarized (see supplementary).

The link between the timing of the recollision events and the resulting selection rules can be quantified. With respect to the case of bi-circular fields, the suppression of the $3m \pm 1$ harmonics corresponds to temporal shifts of the recollisions of only ± 23 attoseconds for the 39th harmonic order. Since a transition of one selection rule (QWP = 45°) to another (QWP = 38°) requires a QWP rotation of 7 degrees, we estimate a timing accuracy of 3.2 attoseconds per degree rotation of the QWP. We believe that this extreme sensitivity of the selection rules will also yield insights into the dynamics of symmetries and chirality in other media, such as crystalline solids. For example, the amount of QWP rotation that is required to reinstate a selection rule provides for a quantitative measure of the symmetry breaking. Although here we used mainly the QWP angle, the same conceptual approach can be applied to experiments with other control parameters.

In conclusion, this work shows experimental evidence for the existence of a triad of three-fold symmetries in high-harmonic spectra, comprised of one known dynamical symmetry and two emergent bandwidth-limited symmetries. These symmetries are unified into a generalized symmetry equation, placing the entire triad on an equal footing. Our findings entail both applied and fundamental aspects. First, sources for the additional phase slips and means of control exist in molecular and condensed-matter systems. Second, the sub-cycle sensitivity of this experiment may allow to resonantly access chiral processes in atoms and molecules with unprecedented attosecond precision and a very high signal to noise ratio. Finally, as dynamical symmetries and their breakdown are broad physical phenomena, the concept of bandwidth-limited symmetries can be extended to other areas of physics and chemistry.

Funding

Deutsche Forschungsgemeinschaft (DFG) (SFB755, project C8), Marie Skłodowska-Curie Grant Agreement No. 752533, and the Göttingen campus laboratory AIMS.

Acknowledgments

OK gratefully acknowledges funding from the European Union's Horizon 2020 Research and Innovation Programme under the Marie Skłodowska-Curie Grant Agreement No. 752533. OK and SZ gratefully acknowledge the support of the Campus Laboratory for Advanced Imaging, Microscopy and Spectroscopy (AIMS).

ORCID iDs

Sergey Zayko https://orcid.org/0000-0001-9826-8627
Ofer Kfir https://orcid.org/0000-0003-1253-9372
Eliyahu Bordo https://orcid.org/0000-0002-6881-441X

References

[1] Fausti D *et al* 2011 Light-induced superconductivity in a stripe-ordered cuprate *Science* **331** 189–91
[2] Oka T and Aoki H 2009 Photovoltaic Hall effect in graphene *Phys. Rev.* B **79** 081406
[3] Lindner N H, Refael G and Galitski V 2011 Floquet topological insulator in semiconductor quantum wells *Nat. Phys.* **7** 490–5
[4] Uzdin R, Mailybaev A and Moiseyev N 2011 On the observability and asymmetry of adiabatic state flips generated by exceptional points *J. Phys. A: Math. Theor.* **44** 435302
[5] Doppler J *et al* 2016 Dynamically encircling an exceptional point for asymmetric mode switching *Nature* **537** 76–9
[6] Henneberger W C 1968 Perturbation method for atoms in intense light beams *Phys. Rev. Lett.* **21** 838–41
[7] Matthews M *et al* 2018 Amplification of intense light fields by nearly free electrons *Nat. Phys.* **14** 695
[8] Choi S *et al* 2017 Observation of discrete time-crystalline order in a disordered dipolar many-body system *Nature* **543** 221–5
[9] Zhang J *et al* 2017 Observation of a discrete time crystal *Nature* **543** 217–20
[10] Cotton F A 2003 *Chemical Applications of Group Theory* (New York: Wiley)
[11] Alon O E 2002 Dynamical symmetries of time-periodic Hamiltonians *Phys. Rev.* A **66** 013414
[12] Herzberg G 1945 *Molecular Spectra and Molecular Structure. Vol. 2: Infrared and Raman Spectra of Polyatomic Molecules* (Malabar, FL: Krieger Publishing Company)
[13] Herzberg G 1966 *Molecular Spectra and Molecular Structure. Vol. 3: Electronic Spectra and Electronic Structure of Polyatomic Molecules* (Malabar, FL: Krieger Publishing Company)
[14] Perry M D and Crane J K 1993 High-order harmonic emission from mixed fields *Phys. Rev.* A **48** R4051–4
[15] Frumker E *et al* 2012 Oriented rotational wave-packet dynamics studies via high harmonic generation *Phys. Rev. Lett.* **109** 113901
[16] Neufeld O, Podolsky D and Cohen O 2019 Floquet group theory and its application to selection rules in harmonic generation *Nat. Commun.* **10** 405
[17] Shen Y R 1989 Surface properties probed by second-harmonic and sum-frequency generation *Nature* **337** 519–25
[18] Macias-Romero C, Nahalka I, Okur H I and Roke S 2017 Optical imaging of surface chemistry and dynamics in confinement *Science* **357** 784–8
[19] Fiebig M, Lottermoser T, Fröhlich D, Goltsev A V and Pisarev R V 2002 Observation of coupled magnetic and electric domains *Nature* **419** 818–20
[20] Jiménez-Galán Á, Zhavoronkov N, Schloz M, Morales F and Ivanov M 2017 Time-resolved high harmonic spectroscopy of dynamical symmetry breaking in bi-circular laser fields: the role of Rydberg states *Opt. Express* **25** 22880
[21] Barreau L *et al* 2018 Evidence of depolarization and ellipticity of high harmonics driven by ultrashort bichromatic circularly polarized fields *Nat. Commun.* **9** 4727
[22] Azoury D *et al* 2019 Electronic wavefunctions probed by all-optical attosecond interferometry *Nat. Photon.* **13** 54
[23] Ferré A *et al* 2015 A table-top ultrashort light source in the extreme ultraviolet for circular dichroism experiments *Nat. Photon.* **9** 93–8
[24] Baykusheva D, Ahsan M S, Lin N and Wörner H J 2016 Bicircular high-harmonic spectroscopy reveals dynamical symmetries of atoms and molecules *Phys. Rev. Lett.* **116** 123001
[25] Sivis M *et al* 2017 Tailored semiconductors for high-harmonic optoelectronics *Science* **357** 303–6
[26] Langer F *et al* 2017 Symmetry-controlled temporal structure of high-harmonic carrier fields from a bulk crystal *Nat. Photon.* **11** 227–31
[27] Liu H *et al* 2017 High-harmonic generation from an atomically thin semiconductor *Nat. Phys.* **13** 262–5
[28] Seiffert L *et al* 2017 Attosecond chronoscopy of electron scattering in dielectric nanoparticles *Nat. Phys.* **13** 766–70
[29] Corkum P B 1993 Plasma perspective on strong field multiphoton ionization *Phys. Rev. Lett.* **71** 1994–7
[30] Lewenstein M, Balcou P, Ivanov M Y, L'Huillier A and Corkum P B 1994 Theory of high-harmonic generation by low-frequency laser fields *Phys. Rev.* A **49** 2117–32
[31] Pedatzur O *et al* 2015 Attosecond tunnelling interferometry *Nat. Phys.* **11** 815–9
[32] Gruson V *et al* 2016 Attosecond dynamics through a Fano resonance: monitoring the birth of a photoelectron *Science* **354** 734–8
[33] Itatani J *et al* 2004 Tomographic imaging of molecular orbitals *Nature* **432** 867–71
[34] Kfir O *et al* 2017 Attosecond-precision coherent control of electron recombination in the polarization plane *Conf. on Lasers and Electro-Optics, paper FM3D.2*
[35] Baykusheva D and Wörner H J 2018 Chiral discrimination through bielliptical high-harmonic spectroscopy *Phys. Rev.* X **8** 031060
[36] Long S, Becker W and McIver J K 1995 Model calculations of polarization-dependent two-color high-harmonic generation *Phys. Rev.* A **52** 2262–78
[37] Fleischer A, Kfir O, Diskin T, Sidorenko P and Cohen O 2014 Spin angular momentum and tunable polarization in high-harmonic generation *Nat. Photon.* **8** 543–9
[38] Kfir O *et al* 2015 Generation of bright phase-matched circularly-polarized extreme ultraviolet high harmonics *Nat. Photon.* **9** 99–105
[39] Eichmann H *et al* 1995 Polarization-dependent high-order two-color mixing *Phys. Rev.* A **51** R3414–7
[40] Dorney K M *et al* 2017 Helicity-selective enhancement and polarization control of attosecond high harmonic waveforms driven by bichromatic circularly polarized laser fields *Phys. Rev. Lett.* **119** 063201
[41] Kfir O *et al* 2016 In-line production of a bi-circular field for generation of helically polarized high-order harmonics *Appl. Phys. Lett.* **108** 211106
[42] Yariv A and Yeh P 2007 *Photonics: Optical Electronics in Modern Communications* (Oxford: Oxford University Press)
[43] Milošević D B and Becker W 2000 Attosecond pulse trains with unusual nonlinear polarization *Phys. Rev.* A **62** 011403
[44] Chen C *et al* 2016 Tomographic reconstruction of circularly polarized high-harmonic fields: 3D attosecond metrology *Sci. Adv.* **2** e1501333

[45] Salières P et al 2001 Feynman's path-integral approach for intense-laser-atom interactions Science 292 902–5
[46] Antoine P, L'Huillier A, Lewenstein M, Salières P and Carré B 1996 Theory of high-order harmonic generation by an elliptically polarized laser field Phys. Rev. A 53 1725–45
[47] Milošević D B, Becker W and Kopold R 2000 Generation of circularly polarized high-order harmonics by two-color coplanar field mixing Phys. Rev. A 61 063403
[48] Popruzhenko S V 2018 Coulomb phase in high harmonic generation J. Phys. B: At. Mol. Opt. Phys. 51 144006
[49] Mancuso C A et al 2015 Strong-field ionization with two-color circularly polarized laser fields Phys. Rev. A 91 031402
[50] Milošević D B 2015 Generation of elliptically polarized attosecond pulse trains Opt. Lett. 40 2381
[51] Milošević D B 2015 Circularly polarized high harmonics generated by a bicircular field from inert atomic gases in the p state: a tool for exploring chirality-sensitive processes Phys. Rev. A 92 043827
[52] Medišauskas L, Wragg J, van der Hart H and Ivanov M Y 2015 Generating isolated elliptically polarized attosecond pulses using bichromatic counter rotating circularly polarized laser fields Phys. Rev. Lett. 115 153001
[53] Pisanty E, Sukiasyan S and Ivanov M 2014 High-order-harmonic generation using bicircular fields Phys. Rev. A 90 043829
[54] Pisanty E and Jiménez-Galán A 2017 Strong-field approximation in a rotating frame: high-order harmonic emission from states in bicircular fields Phys. Rev. A 96 063401